Drew University

College of Liberal Arts

Investigating Substrate Inhibition and the Effects of pH in an Aldo-keto Reductase from a Yeast Strain using Electron Withdrawing Substrates

A Thesis in Biochemistry and Molecular Biology

By

Narisa Diana Lee

Submitted in Partial Fulfilment

of the Requirements

for the Degree of

Bachelors in Science

With Specialized Honours in Biochemistry and Molecular Biology

May 2023

Abstract

Aldo-keto reductases (ARKs) are NADPH-dependent oxidoreductases, catalysing the conversion of aldehydes and ketones into alcohols. AKR's have extensive physiological roles due to their high chemo-, enantio- and regio-selectivity, and broad substrate activity. Many synthetic chemical processes require countless steps to achieve a compound of the right enantioselectivity. Through the use of chemoenzymatic synthesis, these processes can proceed much easier, allowing products to be synthesized stereo-selectively under high yield using fewer steps. With numerous biocatalytic applications, people are on a constant look out for AKR's across a wide range of organisms. Previous research investigating the ketoreductase activity using *Saccharomyces cerevisiae* (SC108) extracted from a 45-million-year-old amber successfully characterized AKR163 with the highest expression. In this study, AKR163 was purified to investigate the role of substrate inhibition and the effects of pH on enzyme activity. By analysing the underlying mechanisms in the ordered binding kinetics, the goal of this project was to determine what is causing substrate inhibition. Additionally, defining the pKa value was of interest to determine specific amino acid interactions for potential mutation studies in the future. Enzyme kinetics were accomplished using non-halogenated substrates like Ethyl-4-nitrobenzoylacetate (E4NBA) and Ethyl acetoacetate (EAA). Results from the kinetic runs were compared to halogenated substrates such as Ethyl-4-chloroacetoacetate (E4ClAA) and Ethyl-2-floroacetoacetate (E2FlAA) to decipher the effects of electron withdrawing properties on substrate inhibition. The kinetic parameters including V_{max}, K_M and K_I were closely examined from each run. Results from the pH dependence study from pH 5.99-6.81 were overall inconclusive due to variability seen in the data and high error values associated with each kinetic parameter. Nevertheless, it seems like more potent inhibition was seen at increased pH levels. Despite this, further investigation is required to conclusively determine the relationship between pH changes and substrate

inhibition. On the other hand, the kinetic data investigating substrate inhibition in electron withdrawing compounds demonstrated a clear relationship between electron withdrawing substrates and its effect on substrate inhibition. This was specifically seen with E4NBA, a non-halogenated electron withdrawing compound which exhibited a characteristic substrate inhibition curve. When comparing this data to EAA, a non-halogenated non-electron-withdrawing substrate, it can be seen that substrate inhibition was not observed. Altogether, the kinetic data from this analysis provided a structural basis in understanding the underlying mechanism leading up to substrate inhibition. Moreover, the results gathered throughout this investigation confirmed that substrate inhibition is a known kinetic phenomenon which can occur in halogenated and non-halogenated electron withdrawing compounds.

Table of Contents

List of Figures and Tables

INTRODUCTION

The study of enzymes provides fundamental insight into the diverse range of chemical reactions found in living organisms. Each reaction taking place on a biochemical pathway requires a specific catalyst, making enzymes critical for life. For a viable chemical reaction to proceed, an input of energy is required and needs to be surpassed (Campbell et al. 2018). Without biological catalysts like enzymes, many chemical processes may not take place. Enzymes speed up chemical reactions by lowering the activation energy required to start a reaction. For this reason, they play significant roles in regulating metabolic processes and pathways. Characterized by their high specificity and efficiency, enzymes function in a catalytic cycle, catalyzing reactions without being consumed. Many chemical processes catalyzed by enzymes are therefore reversible, depending on the relative concentrations of reactant versus product (Campbell et al. 2018).

The Aldo-keto reductases (AKR) superfamily consists of several enzymes which catalyses the conversion of aldehydes and ketones into their corresponding alcohols (Figure 1). These enzymes are NADPH dependent oxidoreductases, meaning they catalyse reactions through a constant supply of cofactor such as NADPH (Barski et al. 2008). The reduction of compounds by AKRs proceed in two steps: first, a hydride ion from NADPH is transferred to the carbonyl substrate, and second, the proton incorporated in the solvent reduces the carbonyl into an alcohol (Barski et al. 2008). AKRs are important industrially and have been well-characterized for their broad substrate activity and high stereoselectivity (Kaluzna, Feske, et al. 2004). Additionally, they pose as potential catalysts in the development of many endogenous compounds.

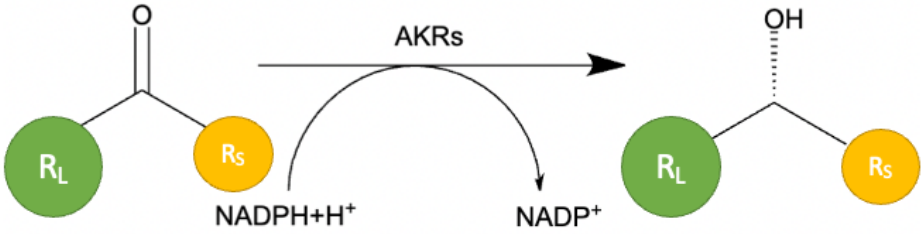

Figure 1. Stereoselective catalysation of Aldo-Keto reductases (AKRs). AKR's catalyse the conversion of carbonyls into alcohols through a constant supply of NADPH, the cofactor.

The development and discoveries of new enzymes has largely been fueled by consumer demands for newer products or industrial attempts to improve existing ones (Kaul and Asano 2011). Although a wide range of enzymes are readily available, their application in chemical synthesis have been limited. Biotechnology and molecular engineering techniques like directed evolution have exploited means to alter the common inadequacies exhibited by enzymes (e.g., problems seen with instability, selectivity, inhibition and low yield). These techniques accelerate the development of more feasible products like therapeutic agents or industrial catalysts (Kaul and Asano 2011). Nevertheless, the employment of these techniques first requires a thorough understanding of the enzyme itself.

In this investigation, AKR163 was analyzed and characterized for its ability to undergo substrate inhibition. Substrate inhibition occurs in a quarter of known enzymes where high levels of substrate concentration cause the rate of reaction to decrease (Wen et al. 2023). This can be an emerging issue for industrial settings as high enzyme activity tends to be favorable and sometimes even required for many large-scale processes. Moreover, enzyme development for the expansion under high substrate concentration may become limited due to

substrate inhibition affecting enzyme productivity (Wen et al. 2023). By investigating the kinetic mechanisms of AKR163, we hope to attain a better understanding of substrate inhibition and potentially, find a way to eliminate it. The first step in understanding many of these biochemical processes begins with enzyme characterization.

The AKR Superfamily

Sequence alignment can reveal important features of AKRs. Understanding the evolutionary pathways of enzymes can be useful, especially for enzyme classification and characterization. Catalytic proteins evolved through billions of years of evolution to keep up with the ever-changing environmental demands. Today, enzymes are able to catalyze a diverse range of chemical reactions using a multitude of substrates due to the improved specificity and functionality acquired over time (Tyzack et al. 2017). In order to attain their new functions, enzymes proceed through various types of changes. Mutations, domain fusions and gene duplication are some of the most common methods seen (Tyzack et al. 2017). In order to identify the evolutionary relationships between homologous enzymes, sequence alignment and structural homologies can be determined.

Sequence alignment and structural homologies are common techniques used to group and identify related proteins under specific families/subfamilies. Carbonyl-reducing enzymes can be grouped into two different enzyme superfamilies - the aldo-keto reductases (AKR) superfamily and the short-chain dehydrogenases/reductases (SDR) superfamily (Hoffmann and Maser 2007). Aldehyde reductases and aldose reductases are examples of some of the most common AKR's seen. According to the protein data bank (PDB), 119 AKR structures and complexes have been identified (Penning 2015). From the 119 AKR structures identified,

16 families were characterized (AKR1-AKR16). Members of AKRs were classified belonging to a different family when less than 40% sequence identity was detected. On the other hand, members were grouped into the same subfamily when more than 60% sequence identity was found (Penning 2015).

As a matter of fact, the AKR superfamily can be found throughout various classes of plants, animals and prokaryotes (Penning 2015). Identifying the sequence homology conserved between these organisms provides a functional basis for understanding enzyme function within a particular family. For instance, a functional genomic study performed using Aldose reductase (AR), an enzyme belonging to the AKR superfamily showed homology was exhibited between human AR and genes from the budding yeast, *Saccharomyces cerevisiae* (Petrash et al. 2001). The study showed that protein residues conserved in the yeast AR-like genes played important catalytic roles in human AR's (Petrash et al. 2001). This demonstrates how yeast functions as a good model organism and can be utilized to study the physiological roles of AKRs. Concordantly, yeast is generally known to sustain manipulations like gene deletions and mutations more readily, making them a desirable system to work with. From identifying the basic kinetic parameters, it was also discovered that all recombinant yeast ARs were in fact NADPH-dependent (Petrash et al. 2001).

As previously mentioned, the AKR superfamily are dependent on nicotinamide cofactors for catalysis. Several studies have shown that most AKRS prefer NADPH over NADH. Through multiple sequence alignments, it has been found that the $(\beta/\alpha)_8$ barrel fold within the structural domain of the protein provides a common scaffold for the NADPH-dependent catalytic activity observed (Jez et al. 1997). Maintaining structural integrity within

the cofactor binding sites can be important as alterations to these sites not only affect enzyme morphology, but also function. Studies have shown similar cofactor binding sites are found retained across AKR subfamilies; even among those exhibiting less than 30% sequence identity (Jez et al. 1997). Using x-ray crystallography, 11 conserved amino acid residues were identified in the primary structure of AKR1C9 (rat liver 3α-hydroxysteroid dehydrogenase) - these include Gly-22, Gly-45, Asp-50, Lys-84, Asp-112, Pro-119, Gly-164, Asn-167, Pro-186, Gln-190 and Ser-271. Five of these residues (Asp-50, Asn-167, Gln-190, Ser-271 and Arg-276) are associated to cofactor binding, while three other residues (Asp-50, Tyr-55 and Lys-84) forms part of the active site (Jez et al. 1997). Determining the structural integrity and specificity of these cofactor binding sites provides a valuable basis for understanding structure-function based relationships. This is particularly useful when considering industrial applications

Stereoselectivity and Substrate Activity for Synthetic Applications

AKRs are known to mediate the stereoselective reduction of prochiral carbonyl compounds producing chiral alcohol enantiomers (Liang et al. 2018). This enantioselective reduction to produce homochiral alcohol is one of the most popular strategies utilized for organic synthesis (Kaluzna et al. 2004). The preparation of optically active alcohols possessing high purity is greatly valued for industrial productions. The ideal catalyst for such conversions would enable broad substrate selectivity, rapid reaction rates and minimal environmental nuisance performed at low cost (Kaluzna et al. 2004). However, steric hindrance is a common issue that arises with bulky substrates, affecting the catalytic behaviour of an enzyme.

To determine the enantioselectivity of AKRs, a research study examined recombinant AKRs from *C. albicans* (CaAKR) against various sterically bulky ketones and ketoesters. Using a gene mining approach, it was found that CaAKR exhibited high catalytic activity and enantioselectivity against bulky ketones, attaining an optical purity of 99% e.e (Liang et al. 2018). However, this was not the only dehydrogenase superfamily illustrating such favourable characteristics – a range of other dehydrogenases and reductases have been well characterized for its ability to sterically reduce bulky substituents. For instance, researchers investigated carbonyl reductase from *Sporobolomyces salmonicolor* (SSCR) and found that the enzyme similarly illustrated stereoselective ketone reduction (Zhu et al. 2006). Sterically bulky ketone substrates such as ethyl 4,4-dimethyl-3-oxopentanoate, ethyl 3,3-dimethyl-2-oxobutanoate and 2-methoxyacetophenone were successfully reduced to their corresponding alcohols, achieving excellent optical purity (Zhu et al. 2006). The configuration and corresponding purity of the resulting enantiomer can determine the value of the biocatalytic molecule in an industrial setting. As a result, the enantioselectivity of an enzyme can be industrially relevant in the production of enantiopure alcohols. For this reason, the ability of AKRs to stereo-selectively reduce a wide range of substrates, particularly, bulky ketones and ketoesters potentially serve as an application-based approach in pharmaceutical productions.

Stereospecificity is a desirable trait for pharmaceutical industries. Another pharmaceutical application seen in AKRs is their role in the chemoenzymatic synthesis of a side chain functional group in statin (Müller 2005). Statins are a well-known LDL-cholesterol lowering drug which aids in decreasing levels of triglycerides in the bloodstream whilst increasing HDL cholesterol – this is particularly important for patients suffering from coronary heart disease. A previous research study has shown that alcohol dehydrogenase, a

novel enzyme belonging to the aldo-keto reductase superfamily played an important role in the stereoselective synthesis of the 3,5-dihydroxy acid side chain, an important functional group found in Statin (Müller 2005). Through various enzymatic transformations, remarkable achievements have been made with the biocatalytic synthesis; these achievements are especially important for applications on an industrial scale

In addition to AKR's having high stereoselectivity, they are also well-recognized for their broad substrate activity. Generally, AKRs are known to be active against a number of steroids, prostaglandins, carbohydrates and lipid aldehydes (Giménez-Dejoz et al. 2015). For example, the human AKR1B15 enzyme was characterized in a research study for its significant activity towards aliphatic and aromatic aldehydes/ketones. Research investigation showed that medium-chain aliphatic and aromatic carbonyls were exceptionally great substrates for this enzyme (Giménez-Dejoz et al. 2015). It is however important to note that enzymes within the same subfamily can have variable activity towards a group of substrates depending on enzyme affinity, substrate specificity and structural properties.

Given the broad substrate activity of AKR's, these reductases tend to have preferential but not mutually exclusive substrate specificity (Kuhn et al. 1995). For instance, D,L-glyceraldehyde and 4-nitrobenzaldehyde are both examples of some of the most common substrates catalyzed by AKR's. While D,L-glyceraldehyde was found to be active towards AKR1B15, this was not the case for AKR1B10, a closely related enzyme also belonging to the AKR1B subfamily (Giménez-Dejoz et al. 2015). Just because a group of substrate exhibits high activity for a specific enzyme, the same concept does not always apply to closely related enzymes in the same subfamily. Overall, understanding the kinetic

properties of an enzyme, specifically its substrate affinities and specificities can be highly important. The kinetic parameters characterized by an enzyme can be applied to various industrial settings to utilize enzymes as potential targets.

Interest in AKRs as Targets

In addition to synthetic applications, AKRs also act as an important target involved in many biochemical reactions. AKRs can be found existing in nearly all phyla including bacteria, fungi, yeast, protozoa, plants, invertebrates, and vertebrates (Jez and Penning 2001). As seen in the previous section, AKRs have been well-characterized for its high chemo-, enantio- and regio-selectivity. They also have a broad substrate activity, enabling them to catalyse a wide range of aldehydes and ketones (Jiang et al. 2021). With their extensive physiological roles, AKR's are important industrially. Numerous pharmacological compounds contain a carbonyl moiety that can be highly reactive. For this reason, pharmaceutical compounds become potential substrates, serving as an important target for AKRs. Examples of some carbonyl-containing drugs reduced by AKRs include bromperidol, benfluron and/or acetohexamide – these are respectively antipsychotic, anti-cancer and antidiabetic class drugs (Barski et al. 2008). Given their ability to catalyse a diverse range of substrates, a common feature seen in AKRs is their ability to perform efficient and rapid detoxification. As a result, glucose, steroids, environmental pollutants, glycosylation end products and lipid peroxidation products are all examples of AKR substrates involved in biosynthesis, metabolism and detoxification (Barski et al. 2008). This trait makes them targets of pharmaceuticals in addition to their use in chemical synthesis.

Research study investigating the role of drug metabolism have shown that human AKRs play significant roles in the detoxification of various pharmaceuticals, drugs and xenobiotics. For example, AKR1B1 (aldose reductase), a crucial enzyme regulating the polyol pathway was found to be a potential mediator in hyperglycaemic injuries (Barski et al. 2008). The polyol pathway is a common metabolic process, used to explain the pathogenesis of diabetes. The two-step pathway involves the reduction of glucose into sorbitol, which in turn gets converted to fructose (Franko et al. 2020). In patients with hyperglycaemia, increased levels of intracellular sorbitol and fructose is often observed, causing osmotic stress and tissue damage. Application of AKR1B1 inhibitors could therefore be implemented to delay or prevent the onset of hyperglycaemic-induced pathologies (Franko et al. 2020). The AKR superfamily, specifically the human AKR1B1 enzyme is thus one of the most promising targets for alleviating diabetic complications.

In addition to the pharmaceutical implications seen in human AKRs, several metabolic applications can also be found using microbial targets. A research study has shown that *Helicobacter pylori* AKR (HpAKR) plays a significant role in the adaptation to acidic pH environments (Cornally et al. 2008). The human pathogen, *H. pylori* is commonly associated to stomach infections like gastritis and ulcerations. By identifying the role and activity of HpAKR in the colonization of *H. pylori* gastric mucosa, researchers were able to characterize HpAKR as a potential therapeutic target for treatment of stomach infections (Cornally et al. 2008). Investigation of the enzyme showed that activity was required for growth under acidic conditions, making them particularly useful for examining biochemical processes under stomach conditions. Again, this demonstrates the functionality of AKRs exhibited across different types of organism. With their wide array of pharmaceutical

importance in mind, researchers have been on a constant lookout for aldo-keto reductases across a wide range of organisms.

Enzyme Kinetics and Substrate Inhibition

Given their importance seen across a number of pharmaceutical applications, AKRs have been subjected for intense study. Understanding the kinetic mechanisms, specifically, the kinetic parameters of AKRs can provide useful insights on how the enzyme functions and interacts with its substrate. In a typical one substrate-enzyme catalyzed reaction, an enzyme binds its substrate to form an enzyme-substrate complex. The enzyme-substrate complex can then be converted to product, while also preserving the enzyme for further recycling (Figure 2). Over time, it is expected that substrate concentration will decrease, while product concentration increase.

$$E + S \underset{k_{-1}}{\overset{k_1}{\rightleftharpoons}} ES \xrightarrow{k_2} P + E$$

Figure 2. A typical one substrate-enzyme catalyzed reaction scheme. In a normal one substrate-enzyme catalyzed reaction, the Michaelis-Menten Kinetics is exhibited.

Substrate specificity of an enzyme is generally deduced using the Michalis-Menten constant (K_M). K_M is inversely related to enzyme affinity; a lower K_M value corresponds to high affinity of an enzyme for its substrate, while a higher K_M indicates low affinity of an enzyme for its substrate (Canela et al. 2019). The Michaelis-Menten kinetic is one of the

most common models used in enzyme kinetics to display the relationship between enzyme velocity and substrate concentration (Le et al. 2019). In the hyperbolic curve exhibited by the Michaelis-Menten model, reaction rates increase linearly with substrate concentration. However, at higher substrate concentrations, reaction velocity reaches a plateau phase, illustrating all active sites on the enzyme have been fully occupied. At this point, the enzyme has reached maximum velocity and increasing substrate concentration will not increase reaction rate any further. The Michaelis Menten kinetic can be visualized using a mathematical equation (Equation 1). The equation describes the rate of enzymatic reactions by relating the initial reaction rate (V_o), the maximum reaction rate (V_{max}), substrate concentration ([S]) and the Michaelis constant (K_M) (Le et al. 2019).

(Equation 1) $$V_0 = \frac{Vmax[S]}{K_M + [S]}$$

This equation is typically used to describe how a rate of reaction is dependent upon its enzymatic concentration and substrate, demonstrating enzymes as useful biocatalytic tools for enhancing catalysis. The Michaelis-Menten equation is particularly useful for investigating the underlying mechanism during catalysis. For instance, the V_{max} measures the maximal reaction velocity, indicating when the enzyme becomes fully saturated with its substrate – this helps characterize how efficient an enzyme is in catalyzing a reaction. Understanding the Michaelis-Menten equation (Equation 1), specifically kinetic parameters can provide useful quantitative implications on how an enzyme functions and its behavior towards various substrates. It is however important to note that not all enzymes follow the typical Michaelis-Menten kinetics – AKR's specifically is one that falls under this category.

Although most enzymes follow the typical Michaelis-Menten kinetics, AKR's follow a phenomenon known as substrate inhibition (Penning et al. 2018). With substrate inhibition, a bi-bi reaction (Figure 3) is seen as opposed to a typical one-substrate enzyme catalyzed reaction (Figure 2). The sequential ordered bi-bi reaction is characterized by the cofactor binding first but leaving last (Figure 3) (Penning 2015). The mechanism begins with the enzyme first binding to NADPH, the cofactor. This results in conformational changes to the protein structure, allowing a substrate to then bind. After the substrate binds, the enzyme-cofactor-substrate complex is converted to product, before the product is subsequently released (Penning et al. 2018). In a normal enzyme-catalyzed reaction, the cofactor usually leaves after the product leaves. However, in this ordered binding mechanism, the cofactor remains bound to the enzyme. This allows time for a second substrate to enter and bind to the complex, resulting in substrate inhibition (Figure 4, model 1).

$$E + C \leftrightharpoons E \bullet C + S \leftrightharpoons E \bullet C \bullet S \leftrightharpoons E \bullet C^* \bullet P \leftrightharpoons E \bullet C^* \leftrightharpoons E + C$$

Figure 3. Bi-bi (ordered binding) reaction mechanisms of AKRs

Substrate inhibition is one of the most common deviations seen from the Michaelis-Menten and occurs in approximately 25% of known enzymes (Kokkonen et al. 2021). It is characterized by the simultaneous binding of two or more substrates molecules, forming an unproductive enzyme-substrate complex (Kokkonen et al. 2021). An enzyme generally contains two binding sites for its substrate – a catalytic binding site and a non-catalytic binding, also referred to as the allosteric site (Reed et al. 2010). The binding of substrates to

both sites lead to the formation of products. However, when a substrate is bound at a non-catalytic site, the product is formed at a reduced rate. In many experimental cases, substrate inhibition can be regarded as a biochemical oddity or experimental annoyance (Reed et al. 2010). Nevertheless, there are several instances where substrate inhibition can be important.

For example, substrate inhibition of acetylcholinesterase (ACHe), an enzyme which degrades acetylcholine (ACH) aids in the enhancement of neural signals between synaptic gaps, allowing for rapid signal termination. At high ACH concentrations, the enzyme (ACHe) is inhibited by the substrate. This negative-feedback loop enables the rate of neurotransmitter degradation in the post-synaptic cleft to slow down, but only accelerate when concentrations of ACH decrease (Reed et al. 2010). This timely mechanism demonstrates the significance of substrate inhibition in raising concentrations of ACH, allowing the effects of neurotransmitters to be prolonged in the synaptic cleft. However, substrate inhibition is Not only important for maintaining integrity of the nervous system, it additionally plays critical roles in regulating various biochemical processes. More specifically, substrate inhibition has been found to play crucial roles in the regulation of ATP during glycolysis (Reed et al. 2010). The activity of phosphofructokinase (PFK), an enzyme found in glycolysis is typically regulated via protein phosphorylation. When high levels of ATP and citrate is formed, PFK is inhibited by these by-products via a feedback loop (Reed et al. 2010). By maintaining equilibrium through substrate inhibition, the rates of ATP consumed vs. produced becomes well-regulated, enabling glycolysis to occur synchronously. Additionally, ATP levels can rise and fall depending upon the supply and demand of the body, ensuring homeostasis is maintained. These examples provide a brief overview on the significance of substrate inhibition and its ability to regulate various biochemical processes.

Substrate Inhibition Models

In order to fully understand the roles of substrate inhibition in biological functions, one must first understand how substrate inhibition exactly occurs. The mechanicalistic basis of substrate inhibition can be visualized using the substrate inhibition model below (Figure 4, model 1). As seen in the model, the production of the enzyme-substrate complex (E • S) results in the formation of products (P). However, an enzyme that binds two substrate molecules (S • E • S), one at the active site and one at the inhibitory site results in substrate inhibition (Figure 4, model 1). In other words, the enzyme displays activity when one substrate is bound, but is inhibited when two substrates are bound.

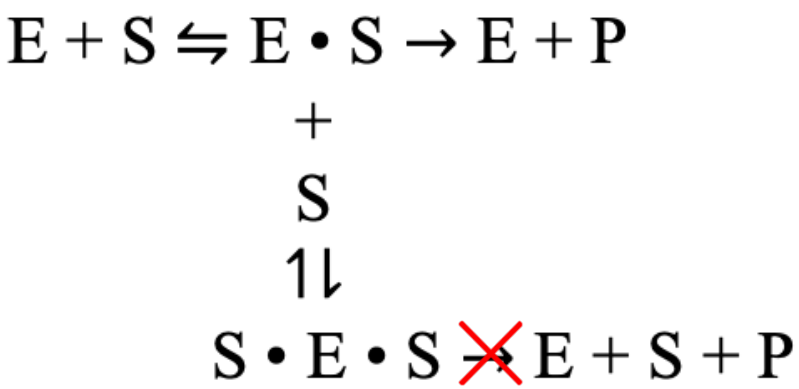

Figure 4. A reaction scheme for the Substrate Inhibition model

(Model 1)

With this being said, it is important to note that inhibition is not always complete. Partial substrate inhibition can sometimes be observed when an enzyme-substrate complex is broken down at a reduced rate (Yoshino and Murakami 2015). Regardless, the binding of a second substrate molecule generally results in lower activity (Reed et al. 2010). Substrate inhibition can be depicted using a characteristic substrate inhibition curve which typically

differs from the hyperbolic curve observed in a Michaelis-Menten reaction. With substrate inhibition, reaction velocity first rises to a maximum, increasing linearly with substrate concentration. However, at very high substrate concentrations, velocity reaches a peak but descends to a zero asymptote (Yoshino and Murakami 2015).

The substrate inhibition model can similarly be depicted using a mathematical equation which relates various kinetic parameters including V_{max}, K_M and K_i (Equation 2). According to the equation, reaction velocity goes to zero as substrate concentration [S] increases. A possible explanation for this could be due to a surplus of enzymes being held up in the unproductive ternary complex when concentration increases, leading to reduced enzyme velocity. Concordantly, the equation takes into account the inhibitor constant, K_i, also sometimes regarded as the dissociation constant for the inhibitory substrate. This parameter is particularly important as it indicates the binding affinity of an enzyme to its inhibitor. More specifically, it illustrates the concentration in which a ligand binds to an enzyme causing reduced catalytic activity. A smaller K_i is generally attributed to a greater inhibition potency, whilst a larger K_i indicates lower inhibition potency. Overall, the mathematical model serves as a great quantitative tool used for characterizing enzyme function. It can potentially be used to understand the underlying mechanism within catalysis by relating different kinetic parameters.

(Equation 2) $$V_0 = \frac{V_{max}[S]}{K'_M + [S] + \frac{[S]^2}{K_i}}$$

While substrate inhibition is generally modelled in conjunction to the Michaelis-Menten mechanism (Figure 4, model 1), other models have concordantly been reported to attribute a possible explanation behind this phenomenon. For instance, one model suggested substrate inhibition occurring as a result of adduct formation in the enzyme-cofactor-substrate complex (Figure 5, model 2). On the other hand, another model indicated substrate inhibition occurring as a result of an alternative binding site (model 3).

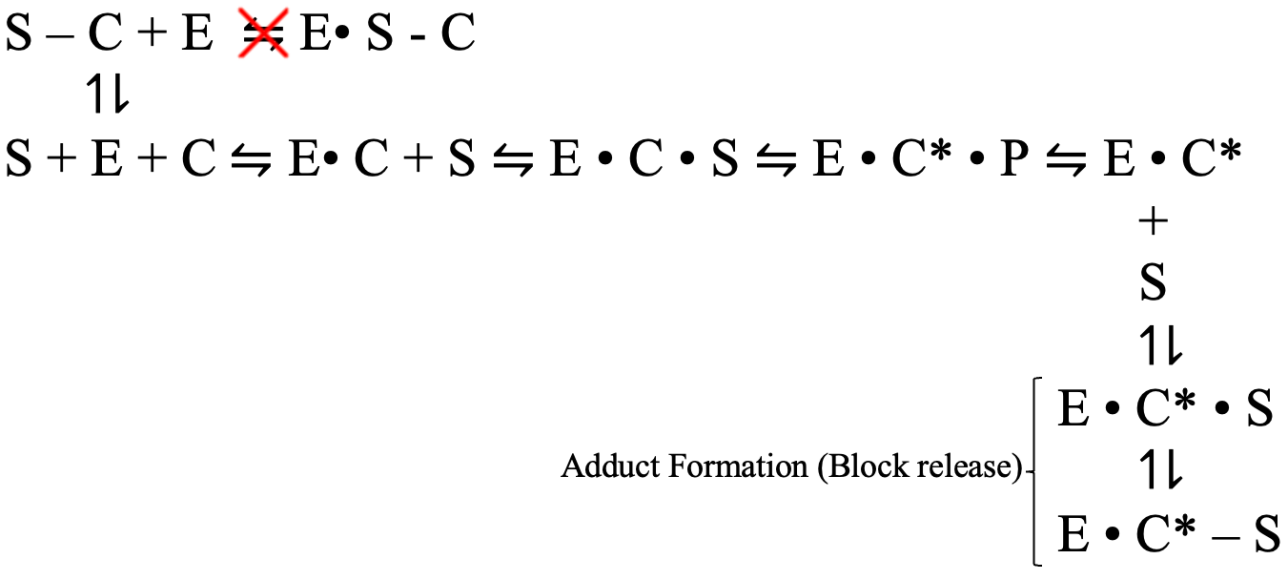

Figure 5. Adduct Formation Substrate Inhibition

(Adapted from Grimshaw et al. 1990b) (Model 2)

Starting with the adduct formation model, a previous paper investigating the nonlinear kinetics of aldehyde reduction by Aldose reductase (ALR-2) demonstrated that the formation of the dead-end E•C•S complex, combined with the formation of the cofactor-substrate adduct lead to a rapidly reversible inhibition (Grimshaw et al. 1990b). In simpler terms, the model indicated that aldose reductase was able to catalyze the formation of a covalent adduct,

resulting in a dead-end complex, and consequently, inhibition (Figure 5, model 2). Note that this model still lies in conjunction with the Michalis-Menten model. The main difference here is that substrate interaction in the enzyme-cofactor complex is held strictly through covalent interactions as opposed to the non-covalent interactions seen in model 1. By using spectroscopic measurements to detect changes in absorbance and fluorescence, it was found that adduct formation occurred between the oxidized form of the cofactor ($NADP^+$) and glycolaldehyde, the substrate examined (Grimshaw et al. 1990b). It was rationalized that glycolaldehyde enol, reversibly formed by 2 and 3 carbon aldehydes was the reactant leading to the formation of the E•C-S adduct complex, explicitly found to occur on the active site of the enzyme (Figure 5, model 2). At high glycolaldehyde concentrations, the enzyme displayed saturation due to competition between the substrate and enol for the enzyme cofactor complex. Interestingly, the ALR-2 mediated adduct formation was enhanced by 79,000-fold relative to the reaction with $NADP^+$ (Grimshaw et al. 1990b). The kinetic evidence gathered from this paper provides a mechanicalistic basis for understanding substrate inhibition, indicating the possibility of adduct formation being the cause of this phenomenon.

Although the previous model indicated substrate inhibition happening as a result of adduct formation, other models have suggested otherwise. A previous research paper examining the crystal structure of the human Δ4-3-Ketosteroid 5β-reductases (AKR1D1-3) revealed the presence of an alternative binding site on the enzyme and hypothesized that this site is attributed to the substrate inhibition observed (Faucher et al. 2008) (model 3). Kinetic characterization of AKR1D1-3 revealed that high enzymatic activity was exhibited towards steroid hormones with the ability to catalyse these substrates in a stereospecific manner.

Nevertheless, substrate inhibition was exerted with progesterone and androstenedione when the concentration of these substrates was twice the K_M value (Faucher et al. 2008). Crystal structures of the enzyme forming a ternary complex with NADPH and androstenedione demonstrated a subsite was present within the enzyme with androstenedione was found in this site. It was proposed that inhibition was caused by the substrate binding to in the alternative site, completely blocking passage of another substrate molecule towards the catalytic site (Faucher et al. 2008). While the crystal structure proposed in this study provides an alternative explanation for substrate inhibition, a contradiction between this alternative binding model is seen relative to the adduct formation model. In the previous model, the substrate and cofactor were bound explicitly to the active site. On the other hand, this model revealed the presence of an alternative site in which the substrate alternatively binds to. For this reason, it is possible that different mechanisms are exerted by different enzymes. Nevertheless, further investigation into enzyme kinetics would be required to be able to fully deduce such conclusions.

Effects of pH on Catalytic Behaviour

Further investigation into the kinetic mechanisms of substrate inhibition showed that this phenomenon occurs in different ways, and various factors including temperature and pH may influence level of inhibition (Grimshaw et al. 1995). Enzyme activity is generally known to be affected by pH, temperature, concentration, and substrate. Since enzymes are made of proteins, they are extremely sensitive to variations in environmental conditions. Enzymes therefore have an optimal range in which they function best. Drastic changes in conditions outside the optimal range can lead to enzyme denaturation or diminished activity (Robinson 2015). Changes in pH takes into account the amount of hydrogen ions present in a solution –

extreme levels of hydrogen ions may result in denaturation of enzymes. For this reason, the maximal rate of enzymatic reactions will be reached only at the optimal pH (Robinson 2015). The optimal range for most enzymes has been found to be around pH 6-8, nevertheless, a few enzymes exhibit an optimum outside this range. It is also important to note that changes in pH not only effect enzyme activity, but also affect the shape and charge of a substrate (Robinson 2015). Therefore, understanding the pH dependence activity displayed by enzymes can be useful in characterizing an pKa value. The pKa value plays an important role in defining the pH dependence characteristics of an enzyme – it can also be useful in understanding the functionality of an enzyme, particularly how we can use it for future applications (i.e., as potential inhibitors to eliminate substrate inhibition).

In a previous investigation on purifying and characterizing an Aldo-keto reductase (AKR-3-2-9) in *Bacillus* sp by researchers from the College of Chemical Engineering in Huquio University, China, it was demonstrated that enzyme's activity and stability varied at different pH's and temperature (Pei et al. 2020). More specifically, it was found that enzyme activity was retained at a relatively broad catalytic pH - the highest activity was observed at pH 6, where 60% activity was maintained at pH 6-8. At pH levels lower than 5.0 and more than 8.0, activity drastically declined. Moreover, reduced activity was seen in sodium citrate and Tris-HCl buffers when compared to sodium phosphate buffers at the same pH level (Pei et al. 2020). This demonstrates evidence for the effects of pH on enzymatic activity. Additionally, this indicates how different buffers influence activity of an enzyme. Therefore, choosing the right buffer for optimal results can be important when performing experiments.

In another study, researchers characterized and purified *S. cerevisiae* (YOL151W) reductase expressed in *E. coli* for the enantioselective production of ethyl-4-chloro-3-oxobutanoate (ECOB) (Choo and Kim 2015). More particularly, the physical and biochemical properties of the immobilized reductase were identified, including the effects of temperature and pH on enzyme activity. The pH-dependence test demonstrated that the optimal pH for both the immobilized reductase and free enzyme was 6.0. Additionally, it was also found that the free enzyme remained stable from pH 4-11 during a 30-minute incubation period, whilst the immobilized enzyme was more stable at pH 11 (Choo & Kim 2015). Again, these results reiterate the effects of pH exerted on enzyme activity. Although evidence here indicate that the optimal pH for different enzymes typically varies, it is important to note that the properties of AKR's from *S. cerevisiae* tend to be similar across a wide range of other aldose reductases found in other microorganisms (Kuhn et al. 1995).

Ketoreductase Activity in Yeast Strain from an Ancient Amber

A research project previously investigated the gene sequence of a 45-million-year-old yeast strain, *Saccharomyces cerevisiae* 108 (SC108) revived from a fossilized amber (Akbary 2019). In the study, ketoreductase activity of the native whole cells were identified and eight AKR's of interest were characterized. From the eight AKR's identified, five were successfully cloned using expression vectors. Concordantly, their stereospecificity and enantioselectivity (R/S isomers) was also determined. All active enzymes were fused to glutathione-S-transferase following the investigation and purified via affinity chromatography. Protein analysis from gel electrophoresis demonstrated AKR163 retaining the highest activity - this can be compared to the other 4 AKRs characterized, demonstrating

lower activity. As a result, the biocatalytic behaviour and enzyme kinetics of AKR163 was further examined.

Current Work

In this study, AKR163 was purified from a yeast strain, *S. cerevisiae* 108 (SC108). The enzyme was characterized and analyzed for its catalytic performance. From examining various substrates including ethyl-4- nitrobenzoylacetate, ethyl acetoacetate, ethyl-2-floroacetoacetate and ethyl-4-chlroacetoacetate (Figure 6) and the basic enzyme parameters, AKR163 demonstrated substrate inhibition with halogenated substrates, consistent with a bi-bi reaction mechanism. Additionally, non-halogenated substrates with electron withdrawing abilities also exhibited substrate inhibition.

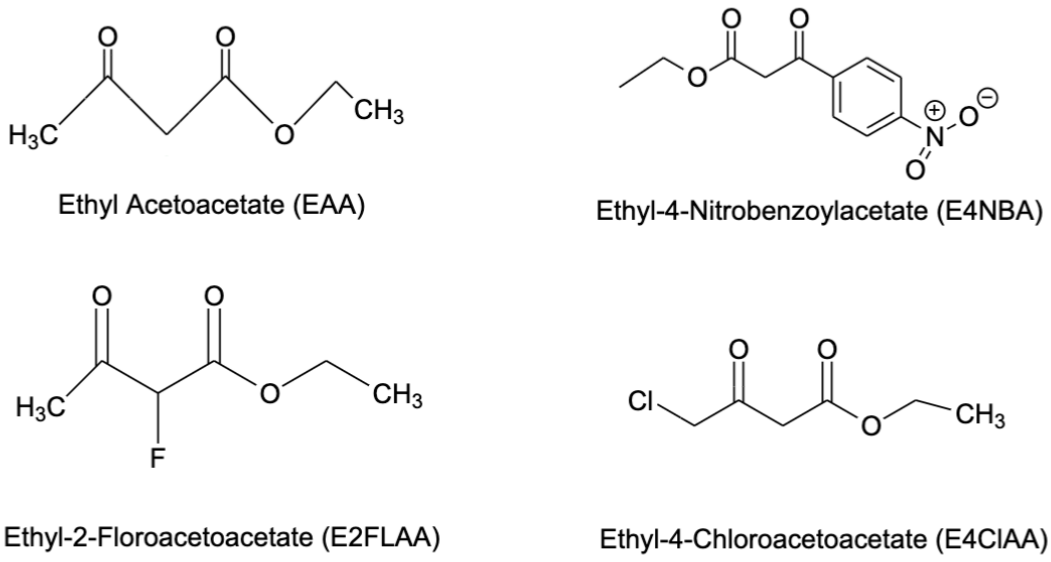

Figure 6. Chemical structures of the four substrates examined in each kinetic run. E2FlAA and E4ClAA are both halogenated substrates with electron withdrawing abilities. EAA and E4NBA are both non-halogenated substrates however, E4NBA contains electron withdrawing groups, EAA do not.

The emphasis of this research project had primarily been focused on studying substrate inhibition and understanding its kinetic behavior. Furthermore, the effects of pH on substrate inhibition in AKR163 was closely examined. In doing so, the goal of the project was to investigate 1) What is causing substrate inhibition? 2) How does substrate inhibition occur? 3) Why does substrate inhibition occur with halogenated substrates? 4) How does pH changes affect the kinetic parameters of an enzyme? It was hypothesized that electron withdrawing group other than halogens will result in substrate inhibition because they are able to speed up the hydride transfer in the forward reaction. In terms of our pH dependence study, it was hypothesized that the protonation of the enzyme substrate complex will speed up the final step of the forward reaction, reducing substrate inhibition. In other words, it was predicted that a decrease in pH, which increases protonation, reduces substrate inhibition.

The hypothesis was deduced from a predicted kinetic model using human aldose reductase recombinant enzyme (Grimshaw et al. 1995). The kinetic model investigated the human aldose reductase using transient kinetic data and rate constants from partial reactions. Interpretation of the kinetic results, particularly the estimated rate constants for reactions using D-xylose and xylitol suggested that the chemical reaction steps involved in the binding of cofactor and substrate to the enzyme proceeds in a fast manner due to hydride transfer which is promoted in the forward reaction – this was supported using rate constants found experimentally through the literature study (Grimshaw et al. 1995). Nevertheless, the step contributing to the conformational change that aids in the release of cofactor (*E•NADPH complex) was found to be the slowest step in the proposed mechanistic model – for this reason, it is very unlikely for the reaction to proceed in the reverse direction once product is released from the complex. With the rate limiting step being characterized in the *E•NADPH

complex, it was hypothesized that a second substrate could come in and bind to the complex leading to inhibition. Additionally, it was also found that a large activation energy is required to overcome the cofactor release, for this reason, the slow rate constants depicted by this complex made sense. With the proposed mechanism, it is also possible that the K_M determined in this experiment may not be indicative of the enzyme's binding affinity to a substrate, but instead useful for examining mechanistic steps in which the enzyme proceeds.

MATERIALS AND METHODS

Making bacterial pellet for protein extraction. In two separate 2L Erlenmeyer flasks, 4.75 g NaCl, 7.75 g Miller's Modified (Luria broth base), 5 mL glycerol, 0.5 mL 1M NaOH was added and dissolved in 500 mL deionized water. This step was repeated in a separate flask, however, 3.1g Miller's Modified (Luria broth base), 1.9 g NaCl, 2 mL glycerol, 0.2 mL 1M NaOH was instead added. The mixture was dissolved using 200 mL deionized water before the mixture was transferred into a 1L KIMAX bottle. The solutions from the 2L Erlenmeyer flasks and 1L KIMAX bottle were autoclaved for 30 minutes at 250°C and left to cool overnight. A 1M IPTG stock solution was then prepared by dissolving 1.025 g IPTG in 4.31 mL deionized water. 1 mL aliquots of the IPTG stock were then transferred into four separate microcentrifuge tubes and stored at -20 °C. Next, a 10 mg/mL Kanamycin solution was prepared in an autoclaved erlenmeyer flask adding 12.5 µL Kanamycin, 25 mL of the 200 mL LB broth solution and 25 µL bacteria (*E. coli*) containing the AKR-163 expression vector. Note that Kanamycin was added to the flask using a 0.2 µm filtered syringe. After mixing, the solution was left to incubate overnight in a shaker at 30 °C for 200 rpm. The resulting solution appeared cloudy, indicating successful bacterial growth. The AKR163 expression vector was made by a previous research student and the protein sequence can be visualized below with the bolded portion indicating all tags from the vector (Akbary 2019).

MGSSHHHHHHGSSMSPILGYWKIKGLVQPTRLLLEYLEEKYEEHLYERD
EGDKWRNKKFELGLEFPNLPYYIDGDVKLTQSMAIIRYIADKHNMLGGCPKER
AEISMLEGAVLDIRYGVSRIAYSKDFETLKVDFLSKLPEMLKMFEDRLCHKTYL
NGDHVTHPDFMLYDALDVVLYMDPMCLDAFPKLVCFKKRIEAIPQIDKYLKSS
KYIAWPLQGWQATFGGGDHPPKGIEENLYFQSNIGSGMSFHQQFFTLNNGNKIPA

IAIIGTGTRWYKNEETDATFSNSLVEQIVYALKLPGIIHIDAAEIYRTYPEVGKALSLTE
KPRNAIFLTDKYSPQIKMSDSPAEGLDLALKKMGTDYVDLYLLHSPFVSKEANGLSL
EEAWKDMEQLYKSGKAKNIGVSNFAVEDLQRILKVAEVKPQVNQIEFSPFLQNQTP
GIYKFCQEHDILLEAYSPLGPLQKKTAQDDSQPFFEYVKELSEKYIKSEAQIILRWVTK
RGVLPVTTSSKPQRISDAQNLFSFDLTAEEVDKITELGLEHEPLRLYWNKLYDKYNY
AAQKV

Concentrating bacterial pellets for protein purification. In the two 500 mL LB broth flasks, 250 µL of 10 mg/mL Kanamycin stock solution previously prepared was added to each flask together with 10 mL of the starter culture. Spectrophotometric readings using a program, Simple Reads at 600 nm absorbance was taken before placing the solutions back onto the shaker for 60 minutes (200 rpm, 30 °C). The samples were taken out and placed back into the shaker periodically to collect spectrophotometric readings at 0-, 60-, 90- and 105-minutes intervals. Once the reading had reached 0.45 absorbance units, 250 µL 1M IPTG was added to both flasks before they were placed back into the shaker for 3 hours (200 rpm, 30 °C). After 3 hours, the bacterial pellet was resuspended using 125mM Tris-HCl, 150 NaCl buffer solution. Once the pellet had been fully resuspended, they were centrifuged for 10 minutes at 4000 rpm using a Beckman GS-6KR. After centrifugation, the supernatant was carefully removed and the pellets were massed before and after to determine the amount of B-PER (Bacterial Protein Extraction reagent) solution needed. The pellets were then stored at -80 °C for protein purification in the next step.

Purification of GST-tagged Protein Using Liquid Chromatography. Using a glutathione column, ten column volumes of 100 µL wash buffer (125 mM Tris-HCl, 150 mM

NaCl) was added for equilibration. 9.7 mL of B-PER solution was added to bacterial pellet #1 for resuspension until homogenously mixed. The resuspended pellet was transferred to the next pellet tube and similarly mixed using a pipette up and down. This was repeated for the remaining pellet tubes, ensuring all pellets were thoroughly mixed before incubation at room temperature for 10-15 minutes. After incubation, the lysate was transferred to a small Nalgene tube for centrifugation at 11,300 rpm for 15 minutes. 200 µL of the lysate was aliquoted into a microcentrifuge tube and stored at -80 °C for referencing purposes. The remaining volume of the solution was added to the equilibrated column and eluted out in 50 mL fractions as the flow through. After so, the column was washed with ten column volumes of 100 µL wash buffer, with five 6 mL fractions and one 20 mL fraction collected using 50 mL tubes. Next, the eluting buffer (125 mM Tris-HCl, 150 mM NaCl, 10 mM reduced glutathione) was added to the column and again, five 6 mL fractions and one 20 mL fractions were collected. Lastly, the column was reconstituted by adding 100 µL of wash buffer, followed by 20% ethanol.

Activity Assay. To detect the proteins from the sample collected, an activity assay was performed using a baseline containing 0.005 M NADPH, 7.400 M E4ClAA (Ethyl-4-Chloro-Acetoacetate), 8 mL pH 8 buffer, 7.28 mL H_2O and 10 µL lysate solution. The solution was transferred into a cuvette and read at 340 nm (180 secs, every 5 secs) using the Ultraviolet-visible spectroscopy (UV-VIS). This was repeated with the remaining solutions collected from the column (WB 1-5 and EB 1-5), with 20 µL of sample used in the baseline instead. With EB 2 and EB 3 exhibiting the highest activity, 6 mL of each solution was aliquoted into the Pierce protein concentrator (PES) tubes before the samples were centrifuged at 3390 rpm for 15 minutes at 3 °C. After centrifugation, the leftover solution was removed from the tube

and reconstituted with buffer volume to make 6 mL. This was repeated for 5 rounds, with centrifugation at 3390 rpm for 20 minutes in the end of every round. After the last centrifugation, buffer was added to the tube to make 6 mL before the sample was stored in the refrigerator at -80 °C.

SDS Polyacrylamide Gel Electrophoresis (SDS-PAGE). To quantify and estimate the molecular weight of the protein collected, an SDS-Gel electrophoresis was performed. SDS-PAGE was performed by preparing a 1:1 mixture of each protein fractions with 25 µL of SDS-denaturing buffer (0.125 M Tris-HCl, pH 6.8, 4% SDS, 20% glycerol, 10% beta-mercaptoethanol, 0.0002% bromophenol blue). The proteins were denatured by placing the samples on a heat block, set at 95 °C for 5 minutes. After so, each sample was placed on ice and loaded into each individual lane. A 200 V was applied to the gel and run using a bromophenol dark blue tracking dye. After the run, the gel was carefully removed from the glass plates and stained using a Coomassie Brilliant Blue Staining Solution. The gel was later de-stained in water/methanol/acetic acid solution and wrapped in a Saran wrap before it was analyzed.

Kinetic Studies. A serial dilution was first performed to obtain varying substrate concentrations – note that a range of concentrations were used for different substrates depending on the initial concentration of the stock solution). To obtain these concentrations, the substrate stock solution was diluted with varying volumes of DMSO, ensuring that the total volume of substrate and DMSO was kept at 2% of the reaction volume. The reaction tubes were set up, each containing 25mM buffer (Tris pH 8-9, MES 5.99-6.81, HEPES 6.81), substrate, 0.10 mM NADPH and Millipore water. The substrate obtained in the reaction tube

came directly from the serial dilutions and ensures varying substrate concentrations were obtained in each reaction. Additionally, the pH ranges examined in this investigation was pH 5.99-6.81 using a 50mM MES buffer. To start the kinetic run, each reaction was transferred into a cuvette and 0.084 μM enzyme was added to each solution before the absorbance was read under using a cary60 UV-VIS at 340 nm for 120 secs (5 sec/cycle and 1 sec average read time). After obtaining data from the kinetic run, data analysis was performed using Excel and Kaleidagraph.

Data Analysis. Each kinetic run from the UV-VIS spectroscopy illustrates the time (seconds) vs. absorbance (Abs/second) at varying substrate concentrations. The data obtained from each kinetic runs were downloaded as a .csv file and imported onto Excel. In Excel, each kinetic run was plotted as a scatter plot and fitted against a linear trend line. Moreover, a line equation was derivatized to identify the slope at each reaction concentration. The slope of the reaction is important for determining the reaction velocity - to determine reaction velocity, the Beer Lambert's Law was applied (Equation 3), using a molar extinction coefficient of -6.22 Ab mM^{-1} cm^{-1} for NADPH at 340 nm. After the initial velocities (in mM/sec) were obtained from each kinetic run, they were plotted against varying substrate concentrations on Kaleidagraph. Using Kaleidagraph, curve fitting was executed by fitting the data to either the Michaelis Menten fit or the substrate inhibition fit (Equation 1 and 2 respectively), yielding values for each kinetic parameters including V_{max}, K_M and K_I. Additionally, R^2 values for each fit were determined to visualize how good of a fit the data was to the model.

(Equation 3) $$A = \varepsilon c l$$

RESULTS

Results from SDS-PAGE

Results from the gel electrophoresis demonstrated a prominent band in lane 7 (elution buffer 2) located at approximately 50-75 kD. This demonstrates that elution buffer 2 contained the highest protein expression relative to the other fractions collected post-purification. Additionally, a faint band can also be observed in the neighbouring lane, coinciding with elution buffer 3, found to be located at approximately the same location. This indicates that some protein expression may also be found in elution buffer 3. For this reason, elution buffer 2 and 3 were the two main fractions utilized to perform our kinetic studies.

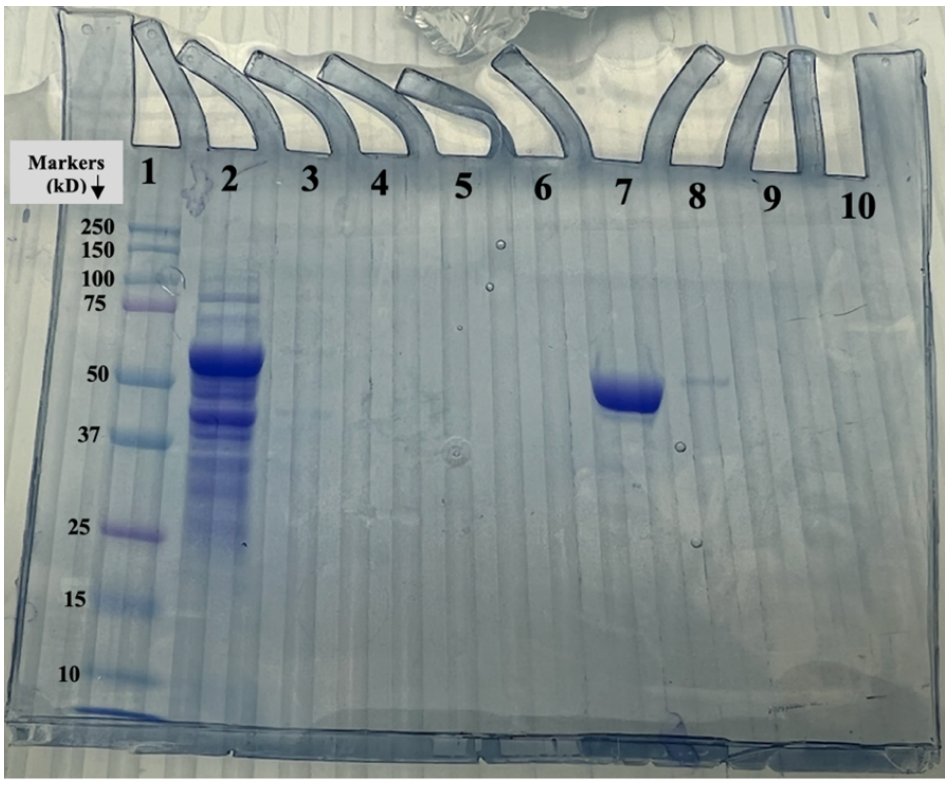

Figure 7. SDS-PAGE of AKR163 protein fractions post-purification. The SDS-PAGE was run under an SDS-denaturing buffer (0.125 M Tris-HCL, pH 6.8, 4% SDS, 20% glycerol, 10% beta-mercaptoethanol, 0.002% bromophenol blue). The gel was stained using Coomassie Brilliant Blue Staining Solution and washed with a water/methanol/acetic acid solution. Lanes are labeled from left to right (1-10) with each lane corresponding to: protein ladder (Precision Plus Protein Dual Color Standards), lysate, wash buffer 2, wash buffer 4, wash buffer 5, elution buffer 1, elution buffer 2, elution buffer 3, elution buffer 4 and elution buffer 5, respectively.

Furthermore, the presence of a distinct band found in lane 7 indicates protein purification was successful. Using the protein ladder in lane 1 and the results obtained from the gel, we can additionally characterize the molecular weight of our purified protein to be 50-75 kD. To confirm this, the protein sequence of AKR163 obtained from a previous research study can be used for comparison, as seen in the methods section (Akbary 2019).

Results from Kinetic Runs

1) Ethyl Acetoacetate

Ethyl acetoacetate (EAA) is a non-halogenated substrate containing no electron withdrawing groups. Results obtained from the kinetic run indicated substrate inhibition was not exhibited. Instead, the enzyme followed the Michaelis-Menten kinetic. For this reason, the data was fitted against a Michaelis-Menten fit, obtaining an R^2 value of 0.99. The fit indicates reaction velocity increasing linearly with substrate concentrations from 10 mM to 168 mM (Figure 8).

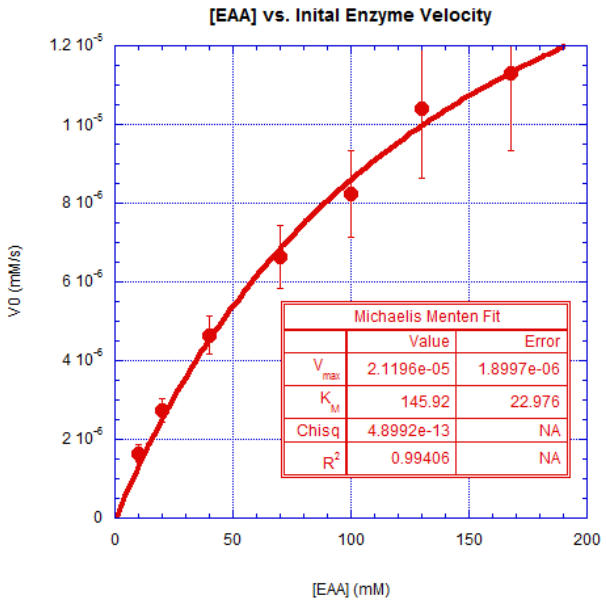

Figure 8. Effects of EAA concentrations on enzyme velocity at pH 8.0. Initial reaction velocity was determined as described in the methods section using the slope and Beer Lambert's law. The data points were fitted on Kaleidagraph using the Michalis-Menten fit, obtaining the kinetic values for V_{max}, K_M and K_I. Data points were taken from an average of 6 kinetic runs with error bars included to show variability in the values.

The V_{max} and K_M obtained from curve fitting were 2.1 x 10^{-5} mM/s and 1.5 x 10^2 mM respectively. Error bars obtained from an average of 6 kinetic trials were additionally included to account for any variability observed in the values. Overall, results indicate that non-halogenated substrates without electron withdrawing groups exhibited a Michaelis-Menten kinetics. This possibly suggests that the presence of an electron withdrawing group within a substrate can be a determining factor affecting whether substrate inhibition is observed or not.

2) Ethyl-4-Chloroacetoacetate

Ethyl-4-chloroacetoacetate (E4ClAA) is a halogenated substrate containing electron withdrawing properties. The kinetic runs performed using this electron withdrawing substrate demonstrated substrate inhibition was exhibited - this can be visualized from the data where a substrate inhibition fit was utilized and the characteristic substrate inhibition curve was consequently observed (Figure 9). Looking more closely into the data, substrate concentration can be seen increasing linearly with reaction velocity. However, at high substrate concentrations (~1000 μM), reaction velocity starts to decline back down. It is also important to note that the data acquired using this substrate was an average obtained from two kinetic runs. The V_{max} and K_M from curve fitting were 8.3 x 10^{-5} μM/s and 7.6 x 10^2 μM respectively. Additionally, the R^2 value from curve fitting was 0.66, indicating a relatively poor substrate inhibition fit. Although the substrate inhibition fit looked fairly poor, the kinetic data was able to show what was expected, which seems to be consistent with previous research done using the same substrate. This indicates results were overall reliable because it was able to repeat previous observations. This therefore gave us confidence to perform

further tests using a non-halogenated electron withdrawing substrate to decipher whether electron withdrawing properties was the main cause of the inhibition observed.

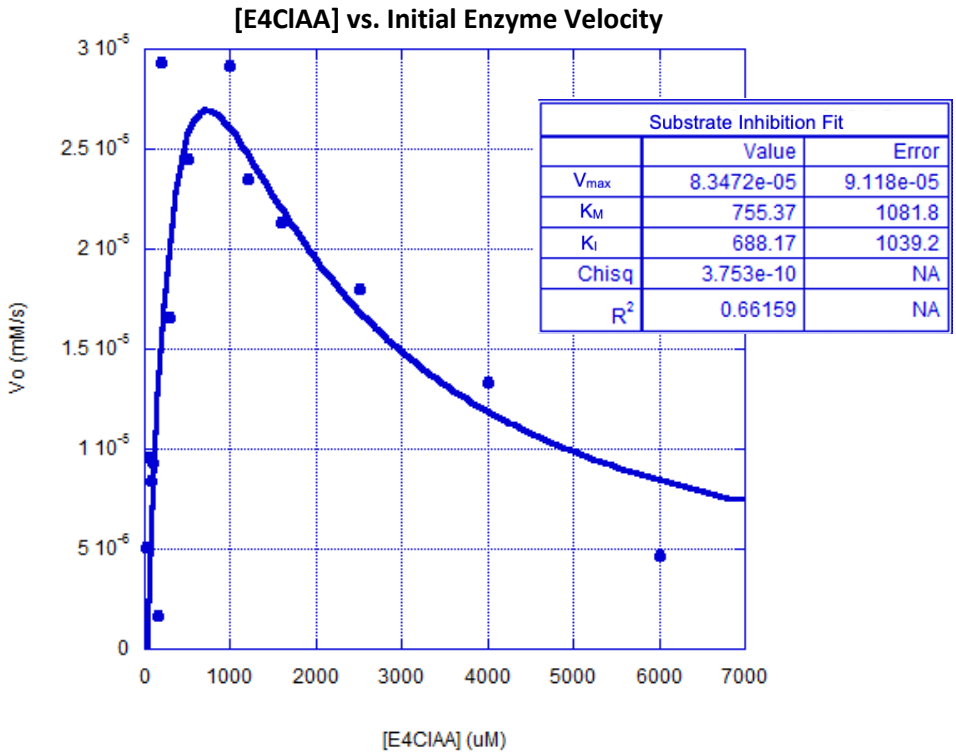

Figure 9. Effects of E4ClAA concentrations on enzyme velocity at pH 6.8. Initial reaction velocity was determined as described in the methods section using the slope and Beer Lambert's law. The data points were fitted on Kaleidagraph using the Michalis-Menten fit, obtaining the kinetic values for V_{max}, K_M and K_I. Data points were taken from an average of 2 kinetic runs.

3) Ethyl-4-Nitrobenzoylacetate

Ethyl-4-nitrobenzoylacetate (E4NBA) is a non-halogenated, electron withdrawing substrate. Substrate inhibition was seen exhibited in the kinetic run performed using E4NBA at pH 9.0 (Figure 10). The kinetic run yielded a characteristic substrate inhibition curve where reaction velocity increases linearly with substrate concentration. However, after some

time, velocity reaches a peak and declines back down. The substrate concentrations examined ranged from 50 µM to 1200 µM. Variability in substrate concentrations were limited by solubility and absorbance of the substrate itself. E4NBA illustrated some level of precipitation and absorption by the substrate at higher concentrations, particularly at 1200 µM. At these concentrations, background signals were observed by the spectrophotometer when NADPH was added. To account for this, the amount of NADPH added was reduced to 10 µL from 20 µL to account for any saturation observed in the reaction mixture. Moreover, the maximum substrate concentration was restricted at 1200 µM because higher concentrations may result in greater instability and absorption.

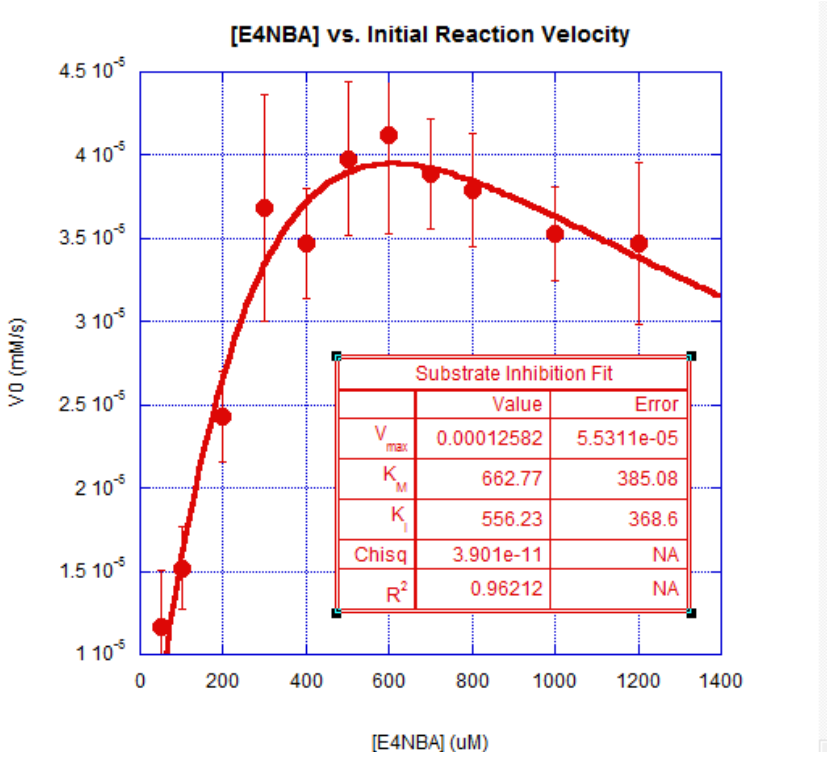

Figure 10. Effects of E4NBA concentrations on enzyme velocity at pH 9.0. Initial reaction velocity was determined as described in the methods section using the slope and Beer Lambert's law. The data points were fitted on Kaleidagraph with a substrate inhibition fit, obtaining the kinetic values for V_{max}, K_M and K_I. Data points were taken from an average of 6 kinetic runs with error bars included to show variability in the values.

The results obtained showed reaction velocity reaching a peak at 4.1 x 10^{-5} mM/s, when substrate concentration is 600 μM (Figure 11). Nevertheless, velocity declines back to 3.5 x 10^{-5} mM/s when substrate concentration doubles. The kinetic parameters Vmax, K_M and K_I obtained from the kinetic run were 1.3 x 10^{-4} mM/s, 6.6 x 10^2 μM and 5.6 x 10^2 μM, respectively. The kinetic data were fitted against a substrate inhibition fit, yielding an R^2 value of 0.96. Variability in the data were accounted for using error bars which were obtained from an average of 6 different trials. The overall results confirm that E4NBA exhibited substrate inhibition – the underlying mechanisms as to how it occurred may be further examined from here.

Results from pH dependence Studies

In order to confirm the effects of pH on substrate inhibition, the halogenated substrates Ethyl-2-Floroacetoacetate (E2FlAA) and Ethyl-4-chloroacetoacetate (E4ClAA) were examined. The kinetic runs performed using E4ClAA confirmed substrate inhibition was exhibited - a characteristic substrate inhibition curve was observed in all the pH levels examined (Figure 11A). However, the effects of pH on levels of inhibition remained unclear as results became fairly scattered with increased pH levels. Although the kinetic data revealed substrate inhibition was prevalent, the results obtained between each pH levels were not clean. The value computed for each kinetic parameters greatly fluctuated and huge error values were obtained (Table 1, 2 and 3) Moreover, curve fitting indicated that the substrate inhibition fit remained poor, yielding an R^2 value as low as 0.44 at pH 6.4 in the unmasked data for the first trial run (Table 1).

With the large variations observed in our data, a second trial run was conducted (Figure 11B). In order to account for any scattering that may be observed, point masking was incorporated into data analysis to eliminate any data points which may seem inconsistent.

Additionally, only data which yielded an R^2 value of 0.95 and above during curve fitting will be taken into consideration in the second trial to ensure a more consistent data.

With these new regulations in mind, a second trial run was conducted from pH 5.99 – 6.81. Results from these runs looked cleaner compared to the first trial run due to point masking (Figure 11A and B). Nevertheless, it was apparent that some degree of scattering was still observed, especially at higher pH's. Although data again confirmed substrate inhibition was prevalent, the substrate inhibition fit did not reach the 0.95 threshold in the unmasked data (Table 2). It was however evident that point masking improved the curve fit in general as R^2 values for the masked data (seen in red) were generally higher than the unmasked data (seen in blue) (Figure 11, Table 2). The highest R^2 value of 0.99 from the second trial run was obtained from the masked data at pH 6.40 relative to the unmasked data, which yielded an R^2 of 0.67 (Table 2). For this reason, the 0.95 R^2 value threshold was only reached when data points were masked in the second trial run at pH 5.99 and 6.4, but still remained below the threshold at pH 6.81. It is also important to note that although point masking did improve the curve fit to some extent, it did not drastically impact the shape of the graph. The substrate inhibition fit obtained from the masked data retained a similar pattern and shape compared to the unmasked data (Figure 11). As a result, point masking remains questionable and averaging was instead resorted. After averaging results from trial 1 and 2, it was evident that the substrate inhibition fit remained poor – there was still a lot of variation seen between each data points for all pH's examined with no improvement in the error values (Figure 11C and Table 3). For this reason, we decided to continue our pH dependence investigation using another electron-withdrawing halogenated substrate, E2FlAA.

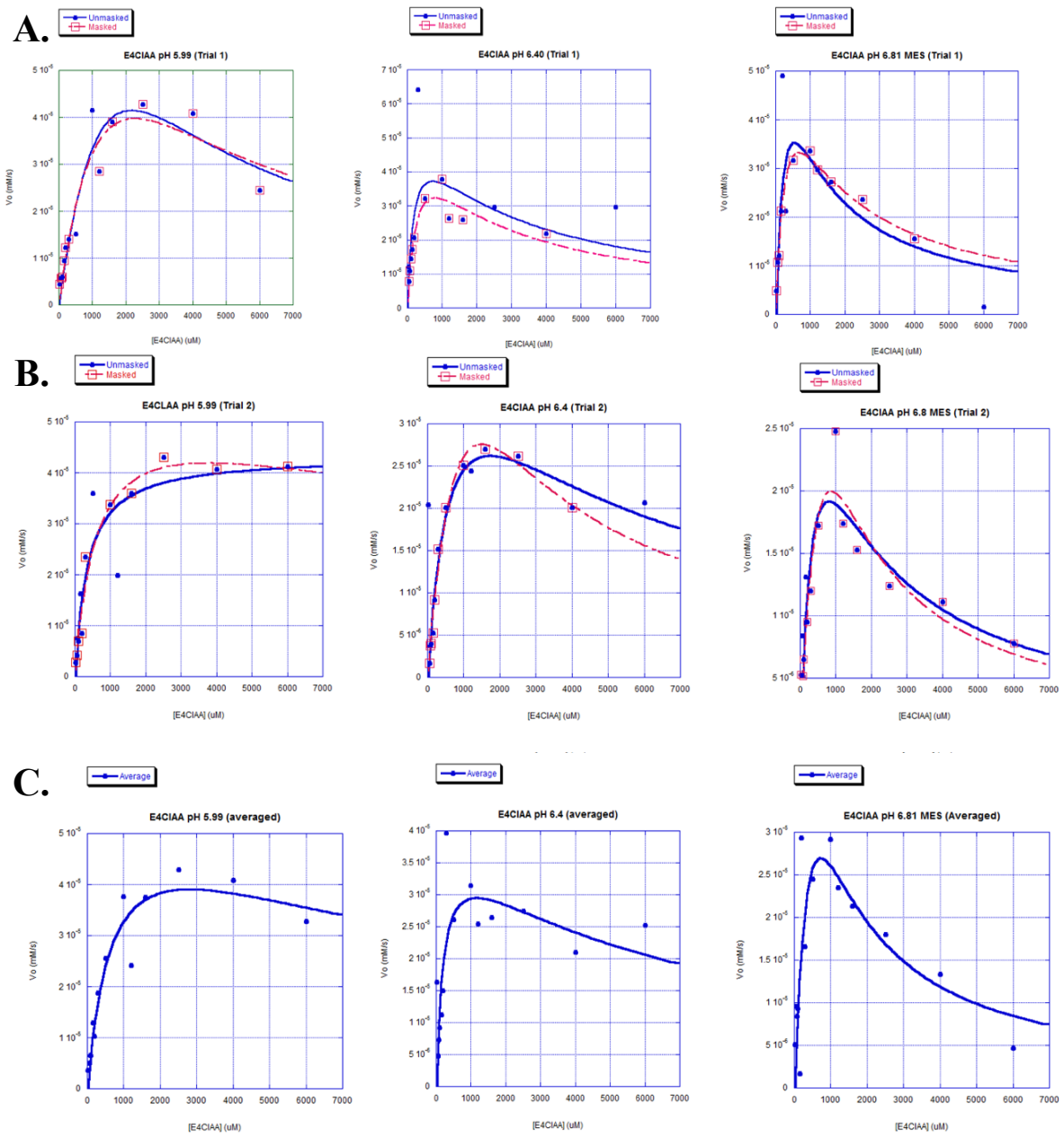

Figure 11. Effects of E4ClAA concentrations on enzyme velocity at pH 5.99 – 6.81. (A) Trial 1 kinetic run with the masked data (in red) and the unmasked data (in blue). (B) Trial 2 kinetic run again showing the masked and unmasked data. (C) Averaged data from Trial 1 and 2 taken using the unmasked data from both trials. Absorbance was taken at 340 nm using the UV-Vis for all trials and data points were fitted onto Kaleidagraph using a substrate inhibition fit.

Table 1. Trial 1 E4ClAA Kinetic data obtained using pH 5.99-6.81 MES Buffer.

	Unmasked		
pH	**5.99**	**6.40**	**6.81**
V_{max} (mM/s)	(1.7 ± 1.8)E-04	(5.7 ± 2.8)E-05	(7.8 ± 5.6)E-05
K_M (µM)	(3.5 ± 4.4)E03	(1.9 ± 1.9)E02	(3.2 ± 3.5)E02
K_I (µM)	(1.4 ± 1.9)E03	(2.9 ± 3.4)E03	(0.90 ± 1.0)E03
R^2	0.92	0.44	0.65
	Masked		
V_{max} (mM/s)	(1.1 ± 0.62)E-04	(5.7 ± 1.5)E-05	(6.7 ± 1.1)E-05
K_M (µM)	(2.0 ± 1.6)E03	(3.1 ± 1.3)E02	(0.034 ± 9.0)E04
K_I (µM)	(2.6 ± 2.3)E03	(2.2 ± 1.3)E03	(1.4 ± 0.40)E03
R^2	0.94	0.90	0.98

Table 2. Trial 2 E4ClAA Kinetic data obtained using pH 5.99-6.81 MES Buffer.

	Unmasked		
pH	**5.99**	**6.4**	**6.81**
V_{max} (mM/s)	(4.3 ± 1.5)E-05	(4.6 ± 2.3)E-05	(4.0 ± 1.7)E-05
K_M (µM)	3.4E02 ± 5.1E-13	(6.4 ± 5.6)E02	(4.4 ± 2.9)E02
K_I (µM)	(9.5 ± 0)E20	(4.7 ± 5.4)E03	(1.5 ± 1.1)E03
R^2	0.87	0.67	0.76
	Masked		
V_{max} (mM/s)	(5.5 ± 0.9)E-05	(8.6 ± 2.7)E-05	(7.9 ± 7.0)E-05
K_M (µM)	(6.1 ± 2.1)E02	(1.6 ± 0.63)E03	(1.3 ± 1.4)E03
K_I (µM)	(2.3 ± 2.3)E04	(1.4 ± 0.66)E03	(5.9 ± 6.7)E02
R^2	0.97	0.99	0.86

Table 3. Averaged E4ClAA Kinetic data obtained using pH 5.99-6.81 MES Buffer.

pH	**5.99**	**6.40**	**6.81**
V_{max} (mM/s)	(5.8 ± 1.3)E-05	(4.0 ± 1.2)E-05	(8.4 ± 9.1)E-05
K_M (µM)	(6.8 ± 2.9)E02	(2.0 ± 1.4)E02	(0.76 ± 1.1)E03
K_I (µM)	(1.2 ± 0.93)E04	(6.7 ± 6.9)E03	(0.69 ± 1.0)E03
R^2	0.93	0.59	0.66

The kinetic runs using E2FlAA similarly confirmed substrate inhibition was exhibited as the characteristic substrate inhibition curve was again obtained (Figure 12). The graph from each run demonstrated reaction velocity approaching its peak before declining back down as substrate concentration increased. The mechanistic effects of pH on levels of inhibition however, remained undetermined. This was again due to similar problems seen in E4ClAA regarding how scattered the data points appeared. The scatter observed was especially prominent at pH 6.8 as the substrate inhibition fit evidently looked worst compared to the lower pH's (Figure 12). There was a lot of scatter and variability between each data points, accounting for the poor R^2 values observed at pH 6.8 MES and HEPES (Table 4). Looking at the data, R^2 values were decreasing with increased pH, starting at a 0.99 R^2 value at pH 5.99 and declining down to a 0.78 R^2 value at pH 6.8 HEPES. In addition to the variability seen in the data points at higher pH's, the kinetic values obtained for V_{max}, K_M and K_i also largely fluctuated with increased pH. The largest V_{max} of 2.2 x 10^{-4} mM/s was observed at pH 5.99 before the value dropped and increased at subsequent pH's (Table 4). In regards to K_M and K_I, there also seems to be no correlation seen between the values obtained and the patterns of fluctuations observed between subsequent pH's. In order to account for any errors which may have occurred during the experimental procedure, a second trial run testing pH 5.99 and 6.4 was performed using E2FlAA. The data obtained from these trials similarly indicated large variability and scattering between subsequent pH's. This inconsistency observed in our data limits our ability to draw correlations between pH behaviour and substrate inhibition. While it seems like substrate inhibition becomes less potent at lower pH's and vice versa at higher pH's, further investigation will be required to conclusively determine this. Nonetheless, the effects of halogens on substrate inhibition, particularly whether substrate inhibition will be observed or not can be fully deciphered.

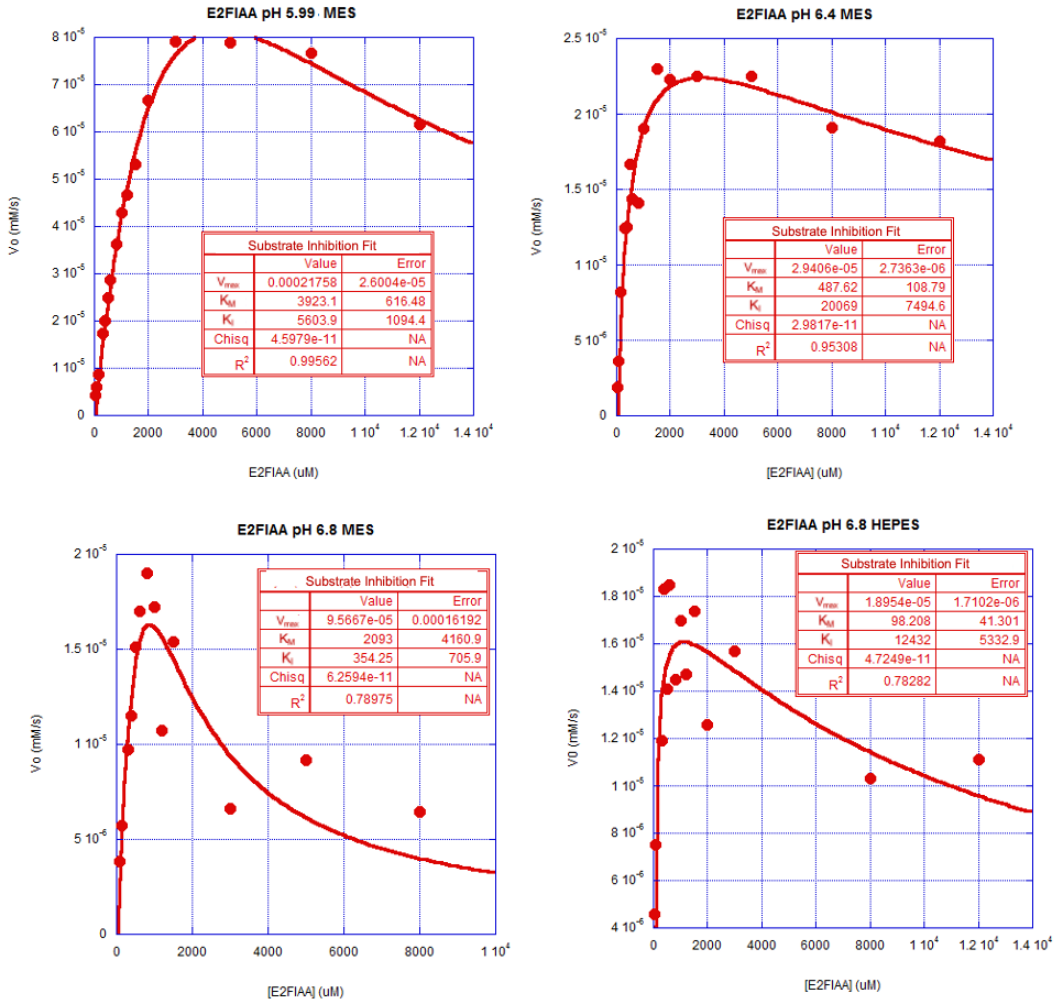

Figure 12. Effects of E2FlAA concentrations on enzyme velocity at pH 5.99-6.81. Kinetic run obtained for E2FlAA using pH 5.99-6.8 MES buffers and a 6.8 HEPES buffer. Initial reaction velocity was determined as described in the methods section using the slope and Beer Lambert's law, taken at 340 nm. The data points were fitted on Kaleidagraph using a Substrate inhibition fit, obtaining the kinetic values for V_{max}, K_M and K_I (Table 4).

Table 4. E2FlAA Kinetic data obtained from pH 5.99-6.81.

pH	5.99	6.40	6.81 MES	6.81 HEPES
V_{max} (mM/s)	(2.2 ± 0.26)E-04	(2.9 ± 0.27)E-05	(0.96 ± 1.6)E-04	(1.9 ± 0.17)E-05
K_M (µM)	(3.9 ± 0.62)E03	(4.9 ± 1.1)E02	(2.1 ± 4.2)E03	(9.8 ± 4.1)E01
K_I (µM)	(5.6 ± 1.1)E03	(2.0 ± 0.75)E04	(3.5 ± 7.0)E02	(1.2 ± 0.53)E04
R^2	0.99	0.95	0.79	0.78

DISCUSSION

In this study, the goal of our investigation was to understand the underlying mechanisms behind substrate inhibition in AKR163. More specifically, we wanted to examine the effects of electron withdrawing substrates and pH. In doing so, some questions we were trying to answer were: 1) What is causing substrate inhibition? 2) How does substrate inhibition occur? 3) Why does substrate inhibition occur with halogenated substrates? 4) How does pH changes affect the kinetic parameters of an enzyme? As previously mentioned, it was hypothesized that electron withdrawing groups will result in substrate inhibition because they are able to speed up hydride transfer in the forward reaction.

From the kinetic runs using non-halogenated substrates, results indicate that electron withdrawing abilities may pose as a factor affecting substrate inhibition. Data from kinetic runs using E4NBA, a non-halogenated substrate with electron withdrawing properties confirmed this (Figure 10). The results from an average of 6 kinetic runs showed substrate inhibition was observed at high substrate concentrations. On the other hand, the kinetic run performed using EAA indicated otherwise – as seen from the graph, the Michaelis-Menten kinetics was instead illustrated (Figure 8). A possible explanation for the differences observed here takes into account the chemical structure of each substrate (Figure 6). Structurally, it can be seen that EAA exhibits less favourable resonance, for this reason, electron withdrawing abilities become limited. Without delocalization of electrons, hydride transfer in the forward direction is not promoted, thus, preventing substrate inhibition from occurring. On the other hand, E4NBA possess electron withdrawing abilities due to the presence of a nitro-group which drives electron withdrawal away from the carbon central, thereby, activating the carbon atom. Once the carbon atom is activated, hydride transfer can be promoted in the forward direction. This subsequently causes substrate inhibition due to an

accumulation of the E•C* complex at high substrate concentrations. This coincides with our hypothesis, as substrate inhibition can be observed in electron withdrawing groups other than halogens.

Although results so far seem to be consistent with our hypothesis and supported by additional data (Grimshaw et al. 1995), it is important to note that some contradictions were found when comparing the results obtained in this investigation from other previous studies. A group of researchers from the University of Orange Free State in South Africa purified and characterized an Aldo-Keto Reductase from *S. cerevisiae,* ARCC 26602 (Kuhn et al. 1995). In this investigation, substrate specificity of the enzyme was tested using aromatic aldehydes and aldoses. Results demonstrated that the enzyme was able to catalyze a wide variety of aldehydes, nevertheless, the best substrate for the enzyme exhibiting high affinity was p-nitro benzaldehyde which was typical for most aldo-keto reductases. (Kuhn et al. 1995). Nevertheless, it was interesting to see that a Michaelis-Menten fit was instead utilized to determine the kinetic parameters as opposed to a substrate inhibition fit. This indicates the enzyme did not exhibit substrate inhibition although the substrate examined was similarly a non-halogenated, electron withdrawing compound. While E4NBA is structurally different from p-nitro-benzaldehyde, it remains true that both these substrates are electron withdrawing compounds. As a result, the inconsistencies observed here remains questionable. This possibly indicates that substrate inhibition may be a phenomenon occurring in specific enzymes, AKR 163 being one of the very few which falls under this category.

To better understand how substrate inhibition is exactly taking place and the underlying mechanisms involved, a reaction scheme examined in a previous research paper can be modelled to illustrate the kinetic steps leading up to inhibition. Using a predicted

model from a previous literature study conducted on the human AR enzyme, it was found that the co-factor release step within the ordered binding kinetic posed as the slowest step in the model (Grimshaw et al. 1995). For this reason, the rate limiting step can be characterized in the E•C* complex (Figure 3). As previously mentioned, electron withdrawing abilities in a substrate promotes hydride transfer allowing the forward reaction to proceed in a fast manner. This means that catalysis of electron withdrawing substrates generally proceeds quickly until the reaction approaches the co-factor release step. With the cofactor release step being rate limiting, an accumulation of enzyme will be held in the E•C* complex (Grimshaw et al. 1995). This enables time for a second substrate to come in and bind to the complex, resulting in inhibition. The predicted model proposed from this research study fits in conjunction to the substrate inhibition model proposed earlier (Figure 4, model 1).

Since electron withdrawal is a property commonly seen with halogenated substrates, the model can be further extended to explain why inhibition was concordantly observed in E4ClAA and E2FlAA. As seen from the kinetic data using E4ClAA and E2FlAA, substrate inhibition was exhibited in both halogenated substrates, yielding the characteristic substrate inhibition curve (Figure 11 and 12). Halogens are characterized by its electronegativity, for this reason, they are known to be electron withdrawing. Using the substrate inhibition model and the predicted model by Grimshaw et. al, the same concept applies – since the substrate is again electron withdrawing, it is expected that substrate inhibition will be observed because an accumulation of enzyme is suspected to be held in the E•C* complex. This suggests how the rate limiting step during the co-factor release plays an important role in the activation of substrate inhibition. Additionally, it gives a structural basis for determining how non-halogenated and halogenated substrates with electron withdrawing properties may exhibit inhibition.

As a matter of fact, this was not the first-time substrate inhibition has been observed in halogenated, electron withdrawing substrates. A previous research paper examining an NADPH-dependent aldehyde reductase (ARII) similarly demonstrated substrate inhibition was observed using ethyl 4-chloro-3-oxobutanoate (4-COBE) (Kita et al. 1999). The velocity studies performed using 4-COBE reduction by wildtype ARII indicated the enzyme was strongly inhibited at high concentrations of 4-COBE (Kita et al. 1999). 4-COBE which we referred to as E4ClAA in our investigation displayed a very similar characteristic substrate inhibition curve to the kinetic runs we performed using E4ClAA. Although it is true that ARII is not an AKR as it belongs under a different reductase family, the results obtained from this study provides insight into the kinetic characteristics of halogenated, electron withdrawing substrates. Additionally, the consistent results observed using the same substrate evidently supports our claim that electron withdrawing substrates consistently exhibit substrate inhibition.

To further support the hypothesis, the kinetic runs obtained using EAA can be utilized for comparison. As seen in the results, substrates that do not contain electron withdrawing abilities like EAA did not exhibit substrate inhibition (Figure 8). Using the substrate inhibition model (model 1), this could similarly be explained by the fact that hydride transfer was not promoted in the absence of delocalized electrons. As a result, the forward reaction will not be promoted. Consequently, this means less accumulation of enzyme will be observed in the rate-determining step, allowing the reaction to proceed smoothly. With the reaction flowing more readily, a second substrate is unlikely to come in and bind to the complex, allowing the reaction to proceed to the end, instead of being held in the *E•C complex. This therefore suggests that without hydride transfer promoted by electron withdrawing groups, no inhibition will be seen. Overall, the findings from this investigation

indicates how structural properties of a substrate can have major impacts on the way an enzyme behaves. More specifically, the results from the data obtained confirms substrate inhibition is a known kinetic phenomenon which occur specifically in halogenated and non-halogenated electron withdrawing substrates.

To confirm the effects of electron withdrawal and its ability to activate substrate inhibition, the kinetic results obtained from this investigation can also be compared to results obtained using another non-halogenated substrate, Ethyl Pyruvate (EPyr). Kinetic runs performed using Ethyl Pyruvate (EPyr) conducted by Paez and Cassano showed substrate inhibition was exhibited. The kinetic data yielded a characteristic substrate inhibition curve with a sharp decrease in reaction velocity at increased substrate concentrations. Looking more closely at the kinetic values, it can be seen that the kinetic runs obtained at pH 7 and 8 yielded very similar values. At pH 8 the V_{max}, K_m and K_I obtained were 1.8 x 10^{-4} mM/s, 0.31 μM and 0.42 μM respectively. It is also important to note here that EPyr is a substrate containing electron withdrawing abilities - the presence of the carbonyl group drives electron withdrawal away from the carbon central. With this in mind, it is therefore possible that substrate inhibition here can similarly be explained by the substrate inhibition model previously discussed (model 1) with electron withdrawal as a the main driving factor.

While data gathered from this investigation remains insufficient to draw conclusions on the exact mechanistic steps leading up to inhibition, the results obtained so far indicates a relationship between electron withdrawing compounds and its effect on substrate inhibition. Further investigation will need to be made regarding the different kinetic parameters, specifically, the rate constants at different points in the reaction to fully examine the mechanistic steps leading up to inhibition.

In terms of the pH dependence studies, it was hypothesized that protonation of the enzyme substrate complex will speed up the final step of the forward reaction, reducing substrate inhibition. In other words, a decrease in pH, which increases protonation, reduces substrate inhibition. Using halogenated substrates, data obtained from the kinetic runs remained inconclusive since a lot of variability was observed between each data points, especially prominent at higher pH's (Figure 11 and 12). Nevertheless, it can generally be seen that substrate inhibition seems less potent at lower pH's. For instance, when examining the kinetic data for E2FlAA, a more potent inhibition can be observed at pH 6.8 relative to pH 5.99 (Table 4).

From examining other pH dependence studies, it has been found that an increase in pH can lead to reduced specific activity. In a previous research study, researchers looked at the pH dependence effects of an aryl-alcohol dehydrogenase (Aad1p) by characterizing its ability to reduce different aldehydes (Yang et al. 2012). Reduction of the recombinant Aad1p enzyme using Veratraldehyde demonstrated the activity of this enzyme was optimal at pH 6.4 (Yang et al. 2012). However, at higher pH's the specific activity of the enzyme declined exponentially. The results obtained from this study seems to coincide with the results obtained in our kinetic runs. Looking back at our results, it is possible that more potent inhibition was observed at higher pH's due to lowered specific activity exhibited by the enzyme. It is also important to note here that in our pH dependence study, we looked at a range of substrate concentrations over a specific pH level at a given time. Contrastingly, the pH dependence study conducted by Yang et al. on Aad1p was done over a single point substrate concentration. As a result, this limits our ability to make any direct comparisons between the variations seen in the kinetic parameters (i.e., V_{max}, K_M and K_I) as pH changes. Additionally, conducting a single point substrate concentration investigation would limit our

ability to see when substrate inhibition is occurring. Regardless, it should still be noted that the kinetic values obtained from our runs demonstrated high error values, indicating low validity in the data obtained (Table 1, 2 and 3)

As previously mentioned, a few changes had been implemented into data analysis to improve data validity – this included point masking and averaging. While point masking improved the substrate inhibition fit to a certain extent, high error values were still observed with little to no change in the shape of the kinetic curves. On the other hand, averaging data from trial 1 and 2 did not seem to improve data validity and reliability either (Table 3). Since data analysis pose as a significant part in this investigation to obtain the kinetic values - the huge variability observed stresses the importance of how we should go about analyzing data. Determining the difference between good and bad data can be challenging, especially when it comes to defining which data points from each kinetic run should be incorporated. Regardless, the factor contributing to these large variations seems to be unknown. For this reason, the effects of pH on levels of inhibition remains uncertain.

Although we have taken the steps to re-evaluate our methods for data analysis, we were still unable to obtain clean data. The high error values and variability seen could in fact be accounted for by various reasons, from systemic errors like mixing the enzyme to possible random errors. Despite the fact, our goal in trying to understand the mechanistic steps for substrate inhibition and its pH dependence effects still remains. Future modifications could be implemented to fully decipher the effects of pH changes on K_I. Nevertheless, the first step in doing so would require a better understanding of the system as a whole. A previous research study has shown that binding of a substrate to the enzyme-NADPH complex may lead to fluorescence enhancement (Nakano and Petrash 1996). This could possibly explain

why huge amounts of scatter was observed in our results. Adding our substrates to the reaction mixture could allow the substrates to interact with the NADPH moiety preemptively, causing intrinsic protein fluorescence and strong absorption (Nakano and Petrash 1996). This strong fluorescence exhibited from the substrate may be a factor interfering with our ability to obtain clean results. This suggests that more controls should be implemented in future studies. Albeit, the variability obtained in our investigation requires more than just averaging and repeating. An in-depth understanding of the system as a whole, including how the substrate interacts with the cofactor and enzyme is substantial for future investigations.

References

Akbary Z. 2019. Ketoreductase activity of 45-million-year-old yeast strains revived from amber [Thesis in Biochemistry and Molecular Biology]. [Drew University].

Barski OA, Tipparaju SM, Bhatnagar A. 2008. The Aldo-Keto Reductase Superfamily and its Role in Drug Metabolism and Detoxification. Drug Metabolism Reviews. 40(4):553–624. doi:https://doi.org/10.1080/03602530802431439.

Campbell NA, Urry LA, Cain ML, Wasserman SA, Minorsky PV, Reece JB. 2018. Biology: a Global Approach. 11th ed. New York Pearson.

Canela EI, Navarro G, Beltrán JL, Franco R. 2019 Apr 13. The meaning of the Michaelis-Menten constant: Km describes a steady-state. Bioxriv. doi:https://doi.org/10.1101/608232.

Choo JW, Kim HK. 2015. Production of (R)-Ethyl-4-Chloro-3-Hydroxybutanoate Using Saccharomyces cerevisiae YOL151W Reductase Immobilized onto Magnetic Microparticles. Journal of Microbiology and Biotechnology. 25(11):1810–1818. doi:https://doi.org/10.4014/jmb.1507.07007.

Cornally D, Mee B, MacDonaill C, Tipton KF, Kelleher D, Windle HJ, Henehan GTM. 2008. Aldo-keto reductase from Helicobacter pylori- role in adaptation to growth at acid pH. FEBS Journal. 275(12):3041–3050. doi:https://doi.org/10.1111/j.1742-4658.2008.06456.x.

Di Luccio E, Elling Robert A, Wilson David K. 2006. Identification of a novel NADH-specific aldo-keto reductase using sequence and structural homologies. Biochemical Journal. 400(1):105–114. doi:https://doi.org/10.1042/BJ20060660. [accessed 2021 Nov 17]. https://www.ncbi.nlm.nih.gov/pmc/articles/PMC1635432/.

Faucher F, Cantin L, Luu-The V, Labrie F, Breton R. 2008. Crystal Structures of Human Δ4-3-Ketosteroid 5β-Reductase (AKR1D1) Reveal the Presence of an Alternative Binding Site Responsible for Substrate Inhibition,. Biochemistry. 47(51):13537–13546. doi:https://doi.org/10.1021/bi801276h.

Franko A, Berti L, Hennenlotter J, Rausch S, Scharpf MO, de Angelis MH, Stenzl A, Birkenfeld AL, Peter A, Lutz SZ, et al. 2020. Transcript Levels of Aldo-Keto Reductase Family 1 Subfamily C (AKR1C) Are Increased in Prostate Tissue of Patients with Type 2 Diabetes. Journal of Personalized Medicine. 10(3):124. doi:https://doi.org/10.3390/jpm10030124.

Giménez-Dejoz J, Kolář MH, Ruiz FX, Crespo I, Cousido-Siah A, Podjarny A, Barski OA, Fanfrlík J, Parés X, Farrés J, et al. 2015. Substrate Specificity, Inhibitor Selectivity and Structure-Function Relationships of Aldo-Keto Reductase 1B15: A Novel Human Retinaldehyde Reductase. Rodrigues-Lima F, editor. PLOS ONE. 10(7):e0134506. doi:https://doi.org/10.1371/journal.pone.0134506. [accessed 2019 Oct 14]. https://www.ncbi.nlm.nih.gov/pmc/articles/PMC4519324/.

Grimshaw CE, Bohren KM, Lai C-J, Gabbay KH. 1995. Human Aldose Reductase: Rate Constants for a Mechanism Including Interconversion of Ternary Complexes by Recombinant Wild-Type Enzyme. Biochemistry. 34(44):14356–14365. doi:https://doi.org/10.1021/bi00044a012.

Grimshaw CE, Shahbaz M, Putney CG. 1990a. Mechanistic basis for nonlinear kinetics of aldehyde reduction catalyzed by aldose reductase. Biochemistry. 29(42):9947–9955. doi:https://doi.org/10.1021/bi00494a027.

Grimshaw CE, Shahbaz M, Putney CG. 1990b. Spectroscopic and kinetic characterization of nonenzymic and aldose reductase mediated covalent NADP-glycolaldehyde adduct formation. Biochemistry. 29(42):9936–9946. doi:https://doi.org/10.1021/bi00494a026.

Hoffmann F, Maser E. 2007. Carbonyl Reductases and Pluripotent Hydroxysteroid Dehydrogenases of the Short-chain Dehydrogenase/reductase Superfamily. Drug Metabolism Reviews. 39(1):87–144. doi:https://doi.org/10.1080/03602530600969440.

Jez JM, Bennett MJ, Schlegel BP, Lewis M, Penning TM. 1997. Comparative anatomy of the aldo–keto reductase superfamily. Biochemical Journal. 326(3):625–636. doi:https://doi.org/10.1042/bj3260625.

Jez JM, Penning TM. 2001. The aldo-keto reductase (AKR) superfamily: an update. Chemico-Biological Interactions. 130-132:499–525. doi:https://doi.org/10.1016/s0009-2797(00)00295-7.

Jiang W, Fu X, Wu W. 2021. Gene mining, codon optimization and analysis of binding mechanism of an aldo-keto reductase with high activity, better substrate specificity and excellent solvent tolerance. PloS One. 16(12):e0260787. doi:https://doi.org/10.1371/journal.pone.0260787. [accessed 2022 Oct 28]. https://pubmed.ncbi.nlm.nih.gov/34855894/.

Kaluzna IA, Feske BD, Wittayanan W, Ghiviriga I, Stewart JD. 2004. Stereoselective, Biocatalytic Reductions of α-Chloro-β-keto Esters. The Journal of Organic Chemistry. 70(1):342–345. doi:https://doi.org/10.1021/jo0484981.

Kaluzna IA, Matsuda T, Sewell AK, Stewart JD. 2004. Systematic Investigation of *Saccharomyces cerevisiae* Enzymes Catalyzing Carbonyl Reductions. Journal of the American Chemical Society. 126(40):12827–12832. doi:https://doi.org/10.1021/ja0469479.

Kaul P, Asano Y. 2011. Strategies for discovery and improvement of enzyme function: state of the art and opportunities. Microbial Biotechnology. 5(1):18–33. doi:https://doi.org/10.1111/j.1751-7915.2011.00280.x.

Kita K, Fukura T, Nakase K-I, Okamoto K, Yanase H, Kataoka M, Shimizu S. 1999. Cloning, Overexpression, and Mutagenesis of the *Sporobolomyces salmonicolor* AKU4429 Gene Encoding a New Aldehyde Reductase, Which Catalyzes the Stereoselective Reduction of Ethyl 4-Chloro-3-Oxobutanoate to Ethyl (*S*)-4-Chloro-3-Hydroxybutanoate. Applied and Environmental Microbiology. 65(12):5207–5211. doi:https://doi.org/10.1128/aem.65.12.5207-5211.1999.

Kokkonen P, Beier A, Mazurenko S, Damborsky J, Bednar D, Prokop Z. 2021. Substrate inhibition by the blockage of product release and its control by tunnel engineering. RSC Chemical Biology. 2(2):645–655. doi:https://doi.org/10.1039/D0CB00171F. [accessed 2021 Nov 5]. https://pubs.rsc.org/en/content/articlelanding/2021/cb/d0cb00171f.

Kuhn A, van Zyl C, van Tonder A, Prior BA. 1995. Purification and partial characterization of an aldo-keto reductase from Saccharomyces cerevisiae. Applied and environmental microbiology. 61(4):1580–1585. doi:https://doi.org/10.1128/aem.61.4.1580-1585.1995.

Liang C, Nie Y, Mu X, Xu Y. 2018. Gene mining-based identification of aldo–keto reductases for highly stereoselective reduction of bulky ketones. Bioresources and Bioprocessing. 5(1). doi:https://doi.org/10.1186/s40643-018-0220-x.

Müller M. 2004. Chemoenzymatic Synthesis of Building Blocks for Statin Side Chains. Angewandte Chemie International Edition. 44(3):362–365. doi:https://doi.org/10.1002/anie.200460852.

Nakano T, Petrash JM. 1996. Kinetic and Spectroscopic Evidence for Active Site Inhibition of Human Aldose Reductase,. Biochemistry. 35(34):11196–11202. doi:https://doi.org/10.1021/bi9608121.

Pei R, Wu W, Zhang Y, Tian L, Jiang W, Zhou S-F. 2020. Characterization and Catalytic-Site-Analysis of an Aldo-Keto Reductase with Excellent Solvent Tolerance. Catalysts. 10(10):1121. doi:https://doi.org/10.3390/catal10101121. [accessed 2021 Nov 18]. https://www.mdpi.com/2073-4344/10/10/1121/htm.

Penning TM. 2015. The aldo-keto reductases (AKRs): Overview. Chemico-Biological Interactions. 234:236–246. doi:https://doi.org/10.1016/j.cbi.2014.09.024.

Penning TM, Wangtrakuldee P, Auchus RJ. 2018. Structural and Functional Biology of Aldo-Keto Reductase Steroid-Transforming Enzymes. Endocrine Reviews. 40(2):447–475. doi:https://doi.org/10.1210/er.2018-00089. https://academic.oup.com/edrv/article/40/2/447/5075994.

Petrash JMark, Murthy BSN, Young M, Morris K, Rikimaru L, Griest TA, Harter T. 2001. Functional genomic studies of aldo–keto reductases. Chemico-Biological Interactions. 130-132:673–683. doi:https://doi.org/10.1016/s0009-2797(00)00258-1.

Reed MC, Lieb A, Nijhout HF. 2010. The biological significance of substrate inhibition: A mechanism with diverse functions. BioEssays. 32(5):422–429. doi:https://doi.org/10.1002/bies.200900167.

Robinson P. 2015. Enzymes: principles and biotechnological applications. Essays in Biochemistry. 59(59):1–41. doi:https://doi.org/10.1042/bse0590001. https://www.ncbi.nlm.nih.gov/pmc/articles/PMC4692135/.

Tyzack JD, Furnham N, Sillitoe I, Orengo CM, Thornton JM. 2017. Understanding enzyme function evolution from a computational perspective. Current Opinion in Structural Biology. 47:131–139. doi:https://doi.org/10.1016/j.sbi.2017.08.003.

Wen Y, Xu J, Pan D, Wang C. 2023. Removal of substrate inhibition of Acinetobacter baumannii xanthine oxidase by point mutation at Gln-201 enables efficient reduction of purine content in fish sauce. Food Chemistry: X. 17:100593. doi:https://doi.org/10.1016/j.fochx.2023.100593.

Yang D, Jean Marie François, Gustavo. 2012. Cloning, expression and characterization of an aryl-alcohol dehydrogenase from the white-rot fungus Phanerochaete chrysosporium strain BKM-F-1767. BMC Microbiology. 12(1). doi:https://doi.org/10.1186/1471-2180-12-126.

Yoshino M, Murakami K. 2015. Analysis of the substrate inhibition of complete and partial types. SpringerPlus. 4(1). doi:https://doi.org/10.1186/s40064-015-1082-8. https://www.ncbi.nlm.nih.gov/pmc/articles/PMC4478191/.

Zhu D, Yang Y, Buynak JD, Hua L. 2006. Stereoselective ketone reduction by a carbonyl reductase from Sporobolomyces salmonicolor. Substrate specificity,

enantioselectivity and enzyme-substrate docking studies. Organic & Biomolecular Chemistry. 4(14):2690. doi:https://doi.org/10.1039/b606001c.